

# Exploring the effects of Delta Baryons in magnetars

Kuan Dalfovo Marquez

*marquezkuan@gmail.com*

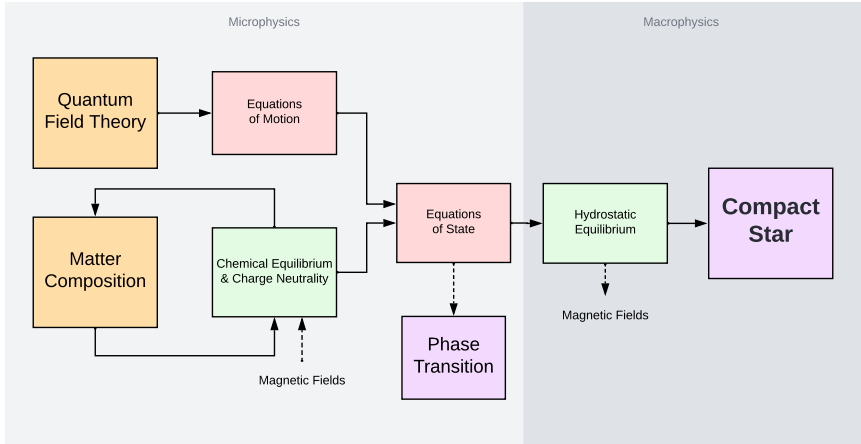


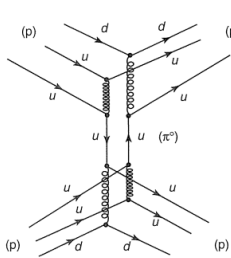
with the collaboration of

D. P. Menezes, V. Dexheimer, D. Chatterjee, M. R. Pelicer and B. C. T. Backes

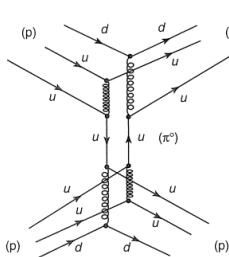
25/10/2022

- DEXHEIMER, V.; MARQUEZ, K. D.; MENEZES, D. P. **Delta baryons in neutron-star matter under strong magnetic fields**. EUROPEAN PHYSICAL JOURNAL A 57 216, 2021. [arXiv:2103.09855]
- BACKES, B. C. T.; MARQUEZ, K. D.; MENEZES, D. P. **Effects of strong magnetic fields on the hadron-quark deconfinement transition**. EUROPEAN PHYSICAL JOURNAL A 57 229, 2021. [arXiv:2103.14733]
- MARQUEZ, K. D.; PELICER, M. R.; GHOSH, S.; PETERSON, J.; CHATTERJEE, D.; DEXHEIMER, V.; MENEZES, D. P. **Exploring the effects of Delta Baryons in magnetars**. PHYSICAL REVIEW C 106 035801, 2022. [arXiv:2205.09827]





$$\begin{aligned}
 \mathcal{L} = & \sum_b \bar{\psi}_b \left[ \gamma_\mu \left( i\partial^\mu - g_{\omega b}\omega^\mu - g_{\phi b}\phi^\mu - \frac{g_{\rho b}}{2}\vec{\tau} \cdot \vec{\rho}^\mu \right) - M \right] \psi_b \\
 & + \frac{1}{2}(\partial_\mu\sigma\partial^\mu\sigma - m_\sigma^2\sigma^2) - \frac{\lambda_1}{3}\sigma^3 - \frac{\lambda_2}{4}\sigma^4 \\
 & - \frac{1}{4}\Omega_{\mu\nu}\Omega^{\mu\nu} + \frac{1}{2}m_\omega^2\omega_\mu\omega^\mu - \frac{1}{4}\Phi_{\mu\nu}\Phi^{\mu\nu} + \frac{1}{2}m_\phi^2\phi_\mu\phi^\mu \\
 & - \frac{1}{4}\vec{R}_{\mu\nu} \cdot \vec{R}^{\mu\nu} + \frac{1}{2}m_\rho^2\vec{\rho}_\mu \cdot \vec{\rho}^\mu + g_{\omega\rho}\omega_\mu\omega^\mu\vec{\rho}_\mu \cdot \vec{\rho}^\mu,
 \end{aligned} \quad (1)$$



$$\begin{aligned}
 \mathcal{L} = & \sum_b \bar{\psi}_b \left[ \gamma_\mu \left( i\partial^\mu - g_{\omega b}\omega^\mu - g_{\phi b}\phi^\mu - \frac{g_{\rho b}}{2}\vec{\tau} \cdot \vec{\rho}^\mu \right) - M \right] \psi_b \\
 & + \frac{1}{2}(\partial_\mu\sigma\partial^\mu\sigma - m_\sigma^2\sigma^2) - \frac{\lambda_1}{3}\sigma^3 - \frac{\lambda_2}{4}\sigma^4 \\
 & - \frac{1}{4}\Omega_{\mu\nu}\Omega^{\mu\nu} + \frac{1}{2}m_\omega^2\omega_\mu\omega^\mu - \frac{1}{4}\Phi_{\mu\nu}\Phi^{\mu\nu} + \frac{1}{2}m_\phi^2\phi_\mu\phi^\mu \\
 & - \frac{1}{4}\vec{R}_{\mu\nu} \cdot \vec{R}^{\mu\nu} + \frac{1}{2}m_\rho^2\vec{\rho}_\mu \cdot \vec{\rho}^\mu + g_{\omega\rho}\omega_\mu\omega^\mu\vec{\rho}_\mu \cdot \vec{\rho}^\mu,
 \end{aligned} \quad (1)$$

Model	$n_0$	$B/A$	$K$	$\mathcal{S}$	$L$	$M/m$
GM1	0.153	16.33	300.5	32.5	94	0.70
$L3\omega\rho$	0.156	16.20	256	31.2	74	0.69
DDME2	0.152	16.14	251	32.3	51	0.57
Constr.	0.148–0.170	15.8–16.5	220–260	28.6–34.4	36.0–86.8	0.6–0.8

**Table:** symmetric nuclear matter properties at saturation density for the models employed in this work.

$$\mu_b = \mu_n - q_b \mu_e \quad (2)$$

$$\sum_{i=b,l} q_i n_i = 0 \quad (3)$$

$$\mu_b = \mu_n - q_b \mu_e \quad (2)$$

$$\sum_{i=b,l} q_i n_i = 0 \quad (3)$$

$$\begin{aligned} \varepsilon = & \sum_b \frac{1}{\pi^2} \int_0^{p_{F_b}} dp p^2 \sqrt{p^2 + M_b^2} + \frac{1}{2} m_\sigma^2 \sigma_0^2 + \frac{\lambda_1}{3} \sigma_0^3 + \frac{\lambda_2}{4} \sigma_0^4 \\ & - \frac{1}{2} m_\omega^2 \omega_0^2 - \frac{1}{2} m_\phi^2 \phi_0^2 - \frac{1}{2} m_\rho^2 \rho_0^2 - g_{\omega\rho} \omega_0^2 \rho_0^2 + \varepsilon_{\text{leptons}}, \end{aligned} \quad (4)$$

$$P = -\varepsilon + \sum_b \mu_b n_b \quad (5)$$

$$\mu_b = \mu_n - q_b \mu_e \quad (2)$$

$$\sum_{i=b,l} q_i n_i = 0 \quad (3)$$

$$\begin{aligned} \varepsilon = & \sum_b \frac{1}{\pi^2} \int_0^{p_{F_b}} dp p^2 \sqrt{p^2 + M_b^2} + \frac{1}{2} m_\sigma^2 \sigma_0^2 + \frac{\lambda_1}{3} \sigma_0^3 + \frac{\lambda_2}{4} \sigma_0^4 \\ & - \frac{1}{2} m_\omega^2 \omega_0^2 - \frac{1}{2} m_\phi^2 \phi_0^2 - \frac{1}{2} m_\rho^2 \rho_0^2 - g_{\omega\rho} \omega_0^2 \rho_0^2 + \varepsilon_{\text{leptons}}, \end{aligned} \quad (4)$$

$$P = -\varepsilon + \sum_b \mu_b n_b \quad (5)$$

$$\frac{dP}{dr} = - \frac{[\varepsilon(r) + P(r)] [m(r) + 4\pi r^3 P(r)]}{r [r - 2m(r)]}, \quad (6)$$

$$m(r) = \int_0^r dr' 4\pi r'^2 \varepsilon(r'). \quad (7)$$

	$M_b$ (MeV)	$q_b(e)$	$I_{3b}$	$S_b$	$\mu_b/\mu_N$	$\kappa_b/\mu_N$
$p$	939	+1	+1/2	1/2	2.79	1.79
$n$	939	0	-1/2	1/2	-1.91	-1.91
$\Lambda$	1116	0	0	1/2	-0.61	-0.61
$\Sigma^+$	1193	+1	+1	1/2	2.46	1.67
$\Sigma^0$	1193	0	0	1/2	1.61	1.61
$\Sigma^-$	1193	-1	-1	1/2	-1.16	-0.37
$\Xi^0$	1315	0	+1/2	1/2	-1.25	-1.25
$\Xi^-$	1315	-1	-1/2	1/2	-0.65	0.06
$\Delta^{++}$	1232	+2	+3/2	3/2	4.99	3.47
$\Delta^+$	1232	+1	+1/2	3/2	2.49	1.73
$\Delta^0$	1232	0	-1/2	3/2	0.06	0.06
$\Delta^-$	1232	-1	-3/2	3/2	-2.45	-1.69

$$g_{ib} = x_{ib} g_i \quad (8)$$

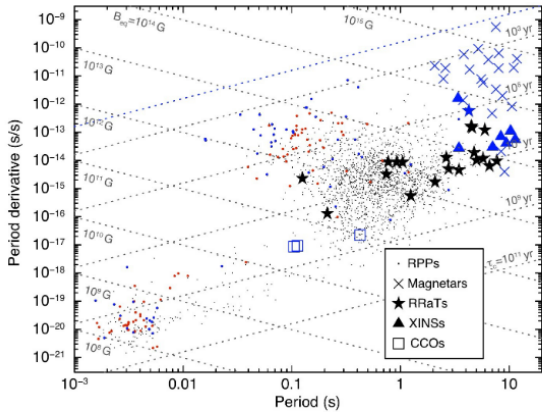


Figure 2 The  $P-\dot{P}$  diagram illustrating the placement of the different isolated neutron star classes. The blue dots mark pulsars detected both in the radio and X-ray bands, the red ones those observed only at X-ray energies. The lines of constant age and magnetic field are also shown (courtesy R.P. Mignani).

$$\int d^3k \rightarrow \frac{|q|B}{(2\pi)^2} \sum_{\nu} \int dk_z, \quad \text{where} \quad \nu = n + \frac{1}{2} - \frac{s}{2} \frac{q_b}{|q_b|} \quad (9)$$

$$\nu_{\max b}(s) = \left\lfloor \frac{(E_{Fb}^* + s\kappa_b B)^2 - M_b^{*2}}{2|q_b|B} \right\rfloor \quad (10)$$

$$\int d^3k \rightarrow \frac{|q|B}{(2\pi)^2} \sum_{\nu} \int dk_z, \quad \text{where} \quad \nu = n + \frac{1}{2} - \frac{s}{2} \frac{q_b}{|q_b|} \quad (9)$$

$$\nu_{\max b}(s) = \left\lfloor \frac{(E_{Fb}^* + s\kappa_b B)^2 - M_b^{*2}}{2|q_b|B} \right\rfloor \quad (10)$$

$q_b = 0$ :

$$k_{F,b}^2(s) = E_{Fb}^{*2} - (M_b^* - s\kappa_b B)^2 \quad (11)$$

$$n_b = \frac{1}{2\pi^2} \sum_s \left\{ \frac{k_{Fb}^3(s)}{3} - \frac{s\kappa_b B}{2} \left[ (M_b^* - s\kappa_b B) k_{Fb}(s) E_{Fb}^{*2} \left( \arcsin \left( \frac{M_b^* - s\kappa_b B}{E_{Fb}^*} \right) - \frac{\pi}{2} \right) \right] \right\} \quad (12)$$

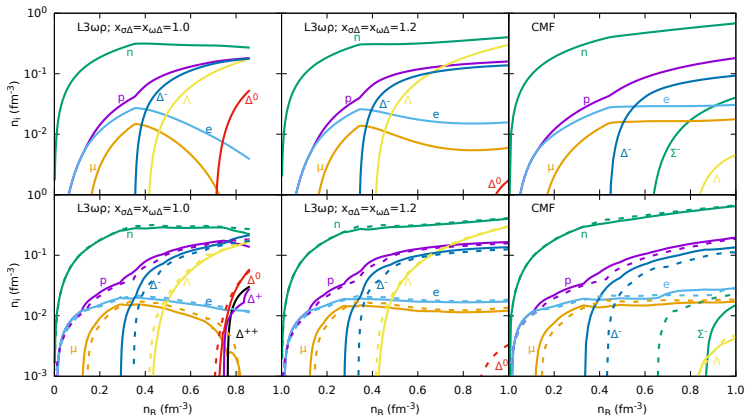
$$n_{sb} = \frac{M_b^*}{4\pi^2} \sum_s \left[ E_{Fb}^* k_{Fb}(s) - (M_b^* - s\kappa_b B)^2 \ln \left| \frac{k_{Fb}(s) + E_{Fb}^*}{M_b^* - s\kappa_b B} \right| \right] \quad (13)$$

$q_b \neq 0$ :

$$k_{F,b}^2(\nu, s) = E_{Fb}^{*2} - \left( \sqrt{M_b^{*2} + 2\nu|q_b|B} - s\kappa_b B \right)^2 \quad (14)$$

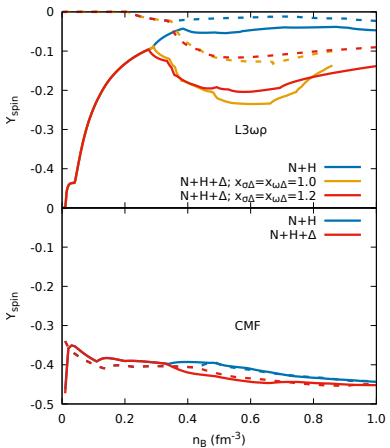
$$n_b = \frac{|q_b|B}{2\pi^2} \sum_{\nu, s} k_{Fb}(\nu, s) \quad (15)$$

$$n_{sb} = \frac{|q_b|B M_b^*}{2\pi^2} \sum_{s, \nu} \frac{\sqrt{M_b^{*2} + 2\nu|q_b|B} - s\kappa_b B}{\sqrt{M_b^{*2} + 2\nu|q_b|B}} \ln \left| \frac{k_{Fb}(\nu, s) + E_{Fb}^*}{\sqrt{M_b^{*2} + 2\nu|q_b|B} - s\kappa_b B} \right| \quad (16)$$

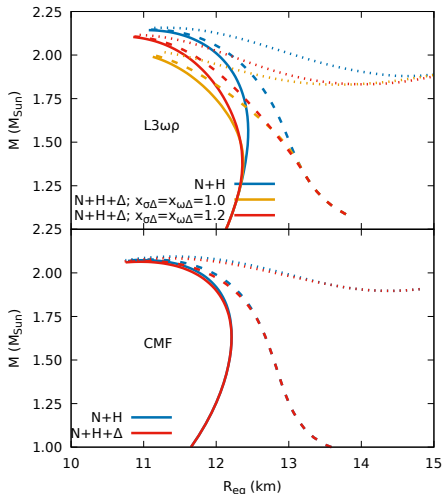


**Figure:** Particle composition of neutron-star matter with  $\Delta$ s, with  $B = 0$  (top panels) and magnetic field  $B = 3 \times 10^{18}$  G (bottom panels), when considering (solid lines) or disregarding (dashed lines) the effects of the AMMs.

$$\gamma_{\text{spin}} = \frac{\sum_{b,s} s n_b(s)}{\sum_{b,s} n_b(s)}, \quad (17)$$



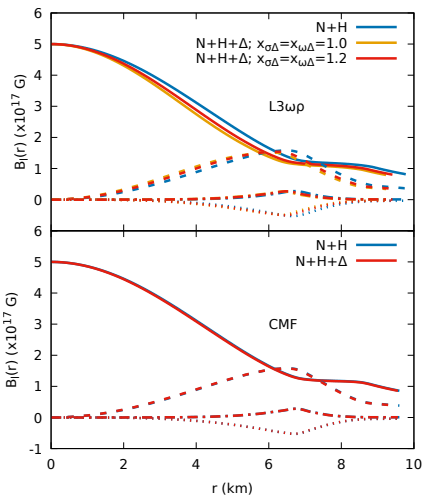
**Figure:** Spin polarization fraction as a function of baryon number density for neutron-star matter with magnetic field  $B = 3 \times 10^{18}$  G, when considering (solid lines) or disregarding (dashed lines) the effects of the AMMs.



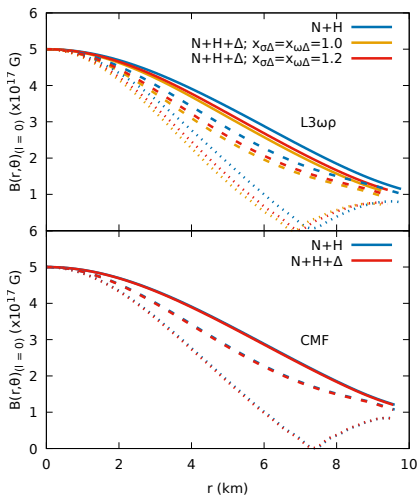
**Figure:** Stellar mass as a function of equatorial radius for different compositions and interaction strengths, for central magnetic fields  $B = 0$  (solid lines),  $B = 5 \times 10^{17}$  G (dashed lines), and  $B = 10^{18}$  G (dotted lines).

$B$ (G)	$n_c$ ( $\text{fm}^{-3}$ )		$\varepsilon_c$ ( $\text{MeV}/\text{fm}^3$ )	
	$N+H$	$N+H+\Delta$	$N+H$	$N+H+\Delta$
0	0.672	0.618 (0.614)	742	658 (657)
$5 \times 10^{17}$	0.701	0.659 (0.653)	783	712 (708)
$1 \times 10^{18}$	0.747	0.714 (0.707)	850	786 (783)
0	0.629	0.625	678	672
$5 \times 10^{17}$	0.680	0.677	747	741
$1 \times 10^{18}$	0.749	0.746	843	837

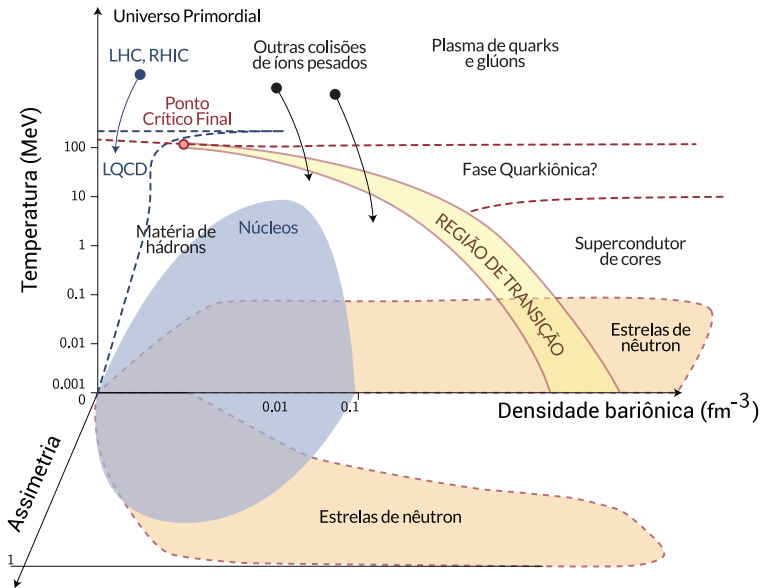
**Table:** Central baryon ( $n_c$ ) and energy ( $\varepsilon_c$ ) densities as a function of magnetic field strength for neutron stars of radius 12 km with  $L3\omega\rho$  model for  $x_{\sigma\Delta} = x_{\omega\Delta} = 1.0(1.2)$  in the top panel and CMF model in the bottom panel.



**Figure:** Magnetic field distribution inside a neutron star of mass  $1.8M_\odot$  and central magnetic field of  $B = 5 \times 10^{17}$  G. Solid, dashed, dashed-dotted and dotted are, respectively, the first four even multipoles of the magnetic field norm ( $l = 0, 2, 4, 6$ ).



**Figure:** Magnetic field distribution inside a neutron star of mass  $1.8M_\odot$  and central magnetic field of  $B = 5 \times 10^{17}$  G. Solid, dashed and dotted are the dominant monopolar ( $l = 0$ ) term at the polar ( $\theta = 0$ ), intermediate ( $\theta = \pi/4$ ) and equatorial ( $\theta = \pi/2$ ) orientations.



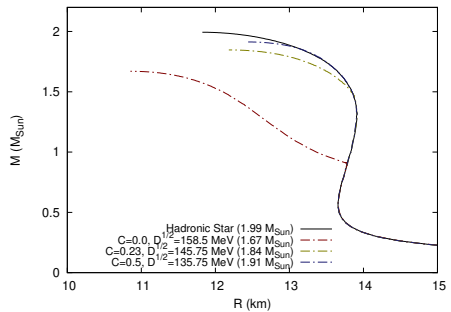


**Figure:** Mass-radius diagram for hybrid EoS with chemical equilibrium in both phases, showing results without magnetic field effects.

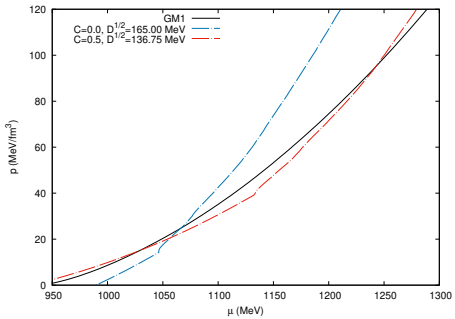


**Figure:** Example of equations of state of parameter choices that allow the hadron-quark phase transition to occur at  $B = 3 \times 10^{18}$  G.

$$m_i = m_{i0} + \frac{D}{n_b^{1/3}} + C n_b^{1/3} = m_{i0} + m_I, \quad (18)$$

	B = 0	B = $3 \times 10^{18}$ G	B-W
C = 0 $\sqrt{D} = 155$ MeV	no crossing	no crossing	yes
C = 0 $\sqrt{D} = 158.5$ MeV	$\mu_0 = 960$ $p_0 = 1.55$	$\mu_0 = 958$ $p_0 = 1.80$	yes
C = 0 $\sqrt{D} = 165$ MeV	$\mu_0 = 1062$ $p_0 = 21.98$	$\mu_0 = 1066$ $p_0 = 24.70$	no
C = 0.23 $\sqrt{D} = 155$ MeV	$\mu_0 = 1130$ $p_0 = 43.62$	$\mu_0 = 1145$ $p_0 = 51.32$	no
C = 0.365 $\sqrt{D} = 142$ MeV	$\mu_0 = 1105$ $p_0 = 34.98$	$\mu_0 = 1109$ $p_0 = 38.30$	yes
C = 0.5 $\sqrt{D} = 135.75$ MeV	$\mu_0 = 1202$ $p_0 = 72.66$	$\mu_0 = 1242$ $p_0 = 94.93$	yes
C = 0.68 $\sqrt{D} = 130$ MeV	$\mu_0 = 1440$ $p_0 = 215.50$	$\mu_0 = 1475$ $p_0 = 247.53$	yes

**Table:** Values for  $\mu_0$  (in MeV) and  $p_0$  (in MeV/fm<sup>3</sup>) for which the conditions of phase coexistence are satisfied at  $T = 0$ . The latter column specifies whether or not the Bodmer-Witten conjecture is satisfied.

- The understanding of the meson-delta coupling parameters can be refined by symmetry group considerations, as it is made for the hyperon coupling schemes.
- The magnetic field effects on  $\Delta$ -admixed matter can be more robustly understood by having the complete solution of the spin-3/2 Rarita-Schwinger equation under a magnetic field.

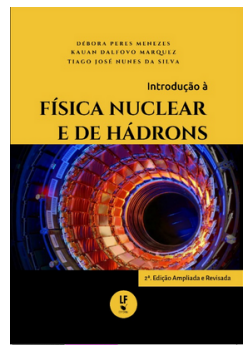
- The understanding of the meson-delta coupling parameters can be refined by symmetry group considerations, as it is made for the hyperon coupling schemes.
- The magnetic field effects on  $\Delta$ -admixed matter can be more robustly understood by having the complete solution of the spin-3/2 Rarita-Schwinger equation under a magnetic field.

**Muito Obrigado!**

Kuan Dalfovo Marquez  
*marquezkuan@gmail.com*



FACULDADE DE  
CIÊNCIAS E TECNOLOGIA  
UNIVERSIDADE FEDERATIVA  
DO RIO GRANDE DO SUL



# Exploring the effects of Delta Baryons in magnetars

Kuan Dalfovo Marquez

*marquezkuan@gmail.com*



with the collaboration of

D. P. Menezes, V. Dexheimer, D. Chatterjee, M. R. Pelicer and B. C. T. Backes

25/10/2022